Relativistic effects in the optical response of HgSe by time- dependent density functionals theory

de Boeij, P.L.; Kootstra, F.; Snijders, J.G.

Published in:
International Journal of Quantum Chemistry

DOI:
10.1002/qua.1516

Relativistic Effects in the Optical Response of HgSe by Time-Dependent Density Functionals Theory

P. L. DE BOEIJ, F. KOOTSTRA, J. G. SNIJDERS

Theoretical Chemistry, Materials Science Centre, Rijksuniversiteit Groningen, Nijenborgh 4, 9747 AG Groningen, The Netherlands

Received 24 February 2001; revised 14 June 2001; accepted 3 July 2001

ABSTRACT: We treat the dominant relativistic effects in the optical response properties of mercury selenide using time-dependent density functional theory (TDDFT). The scalar relativistic effects have been included within the zeroth-order regular approximation (ZORA) in both the ground-state DFT calculations and in the time-dependent response calculations. Within this approximation the HgSe crystal is found to be a semimetal. In a previous study [J Chem Phys 2001, 114, 1860] we have shown that TDDFT/ZORA can be applied successfully to narrow-gap semiconductors, such as indium antimonide, that become semimetallic within the local density approximation when scalar relativistic effects are included. Results are given for the band structure, the static dielectric constant ϵ_∞, and the dielectric function $\epsilon(\omega)$ of HgSe, and these results are compared with the similar ones for InSb. We find considerably improved results for the dielectric function of HgSe when relativistic effects are included. Int J Quantum Chem 85: 449–454, 2001

Key words: relativistic effects; time-dependent functional theory; dielectric function; semimetal; mercury selenide

Introduction

The application of time-dependent density functional theory (TDDFT) for the description of optical properties of crystals [1], in the adiabatic local density approximation (ALDA) yields accurate results for the dielectric constants and optical dielectric functions of various semiconductors and insulators [2]. This approach can also be applied to the case of materials with a vanishing fundamental gap, called semimetals. In a recent work [3] we treated InSb in the zinc blend structure, and we found that the inclusion of relativistic effects resulted in a semimetallic band structure and a greatly improved calculated dielectric function. The deviation from experiment of the calculated dielectric constant was reduced from about 40% in the nonrelativistic calculation to about 5% in the relativistic one.

Recently, the nature of the material HgSe was debated, whether it is a small-gap semiconductor

Correspondence to: P. L. de Boeij; e-mail: p.l.de.boeij@chem.rug.nl.

or a semimetal in the zinc blend structure. Experimentally, as determined using photoemission spectroscopy [4], there seemed to be no evidence of a bulklike conduction band that either crosses or touches the valence-band maximum, hence favoring it to be a small-gap (0.42 eV) semiconductor. On the other hand, conductivity, optical and magneto-optical measurements [5], compiled in Ref. [6], favored an inverted band structure with zero fundamental gap, and thus a semimetallic nature. The seemingly contradicting experimental results have been brought into accordance with an ab initio quasi-particle band structure calculation [7]. This GW calculation (like the DFT-LDA calculation on which it was based) predicts an inverted semimetallic band structure. The experimentally observed very low photoemission intensity just above the valence band maximum could be attributed to the enhanced dispersion, and hence very light effective mass and low density of states, of the lowest conduction band. To our knowledge this GW calculation is the only ab initio study addressing the nature of the material, where other (semi-)empirical calculations [5, 8, 9] cannot resolve the issue since these rely heavily on experimental input parameters.

In this study we show for HgSe that, like in the case of InSb, the inclusion of scalar relativistic effects results in the inverted band structure, with a drastic effect on the optical dielectric constant and the dielectric function.

Theory

Within the framework of ground-state density functional theory (DFT), scalar relativistic effects can be treated using the zeroth-order regular approximation (ZORA) [10–12], in which the kinetic energy operator $p^2/2$ is replaced by its ZORA equivalent, resulting in the following Kohn–Sham equation:

$$\left[\mathbf{p}\cdot\frac{c^2}{2c^2-v_{\mathrm{eff}}(\mathbf{r})}\mathbf{p}+v_{\mathrm{eff}}(\mathbf{r})\right]\psi_{n\mathbf{k}}(\mathbf{r})=\epsilon_{n\mathbf{k}}\psi_{n\mathbf{k}}(\mathbf{r}). \quad (1)$$

Here $\mathbf{p}=-i\nabla$ is the momentum operator, c the velocity of light, and $v_{\mathrm{eff}}(\mathbf{r})$ the self-consistent effective scalar potential. The effective one-electron functions $\psi_{n\mathbf{k}}(\mathbf{r})$ can be found as the solutions of Eq. (1), with eigenvalues $\epsilon_{n\mathbf{k}}$. The ground-state density $\rho_0(\mathbf{r})$ follows from

$$\rho_0(\mathbf{r})=\frac{V}{4\pi^3}\sum_n\int d\mathbf{k}\, f(\epsilon_{n\mathbf{k}})\psi^*_{n\mathbf{k}}(\mathbf{r})\psi_{n\mathbf{k}}(\mathbf{r}). \quad (2)$$

Here the Fermi–Dirac function $f(\epsilon_{n\mathbf{k}})$ selects only those states that have eigenvalues below the Fermi level $\epsilon_{\mathrm{Fermi}}$, and hence only occupied levels contribute to the density.

When the system is perturbed by applying a time-dependent external electric field $\mathrm{E}_{\mathrm{ext}}(\mathbf{r},t)$, the density will become time dependent and currents will be induced, so the system will become polarized. In the time-dependent version of density functional theory, one adds time-dependent vector and scalar contributions to the effective ground-state potential. These additional potentials, respectively, $\mathbf{A}_{\mathrm{eff}}(\mathbf{r},t)$ and $\delta v_{\mathrm{eff}}(\mathbf{r},t)$, have the property that they produce the exact time-dependent density and current of the true system, when applied to the Kohn–Sham system of noninteracting particles. According to the Runge–Gross theorem [13], the time-dependent extension of the Hohenberg–Kohn theory [14, 15], these potentials are, apart from the usual freedom of choice for the gauge, functional of the density and the current, and should therefore be obtained self-consistently. The time-dependent Kohn–Sham system is now obtained by replacing both the ground-state momentum operator by $\mathbf{p}\rightarrow -i\nabla+1/c\mathbf{A}_{\mathrm{eff}}(\mathbf{r},t)$, and the effective scalar potential by the time-dependent version $v_{\mathrm{eff}}(\mathbf{r})\rightarrow v_{\mathrm{eff},0}(\mathbf{r})+\delta v_{\mathrm{eff}}(\mathbf{r},t)$. Within the same order of regular approximation, we can neglect the additional time-dependent contribution to the scalar potential that appears in the denominator of the ZORA kinetic energy term in Eq. (1).

When we neglect the small microscopic contributions to the transverse vector potential (such as the Breit term [16]), we can make a special choice for the gauge, which we will call the microscopic Coulomb gauge [1]. In this gauge both the scalar and vector potential are lattice periodic and have the property that all microscopic components are included in the scalar potential, whereas all macroscopic components are described by the vector potential. The perturbing potentials can be given in this gauge as

$$\mathbf{A}_{\mathrm{eff}}(\mathbf{r},t)=\mathbf{A}(\mathbf{r},t)=-c\int^t dt'\,\mathbf{E}_{\mathrm{mac}}(\mathbf{r},t'), \quad (3)$$

$$\delta v_{\mathrm{eff}}(\mathbf{r},t)=\delta v_{\mathrm{mic}}(\mathbf{r},t)+\int d\mathbf{r}'\,\frac{\partial v_{\mathrm{xc}}[\rho](\mathbf{r})}{\partial\rho(\mathbf{r}')}\bigg|_{\rho_0}\delta\rho(\mathbf{r}',t). \quad (4)$$

Here $\delta v_{\mathrm{mic}}(\mathbf{r},t)$ is the microscopic part of the Hartree potential of the induced density $\delta\rho(\mathbf{r},t)$. In these relations we have neglected any macroscopic contributions of the exchange–correlation (xc) in the vector potential [17], and we used the adiabatic local density approximation (ALDA) for the first-order

xc contribution to the scalar potential. The macroscopic electric field $\mathbf{E}_{\mathrm{mac}}(\mathbf{r}, t)$ is the average field in a region around $\mathbf{r}$ inside the solid, and hence it comprises both the externally applied field $\mathbf{E}_{\mathrm{ext}}(\mathbf{r}, t)$ plus the macroscopic part of the induced field. This latter field is in addition to the induced charge density also due to the induced current density $\delta\mathbf{j}(\mathbf{r}, t)$. We will treat the macroscopic field as the perturbing field, and we will assume that it is uniform and oscillating harmonically with frequency ω, i.e., $\mathbf{E}_{\mathrm{mac}}(\mathbf{r}, t) = \Re\{\mathbf{E}_{\mathrm{mac}}(\omega)\exp(i\omega t)\}$.

The quantity of interest is the induced macroscopic polarization $\mathbf{P}_{\mathrm{mac}}(\omega)$, which will be proportional to this macroscopic field,

$$\mathbf{P}_{\mathrm{mac}}(\omega) = \chi_e(\omega)\cdot\mathbf{E}_{\mathrm{mac}}(\omega). \tag{5}$$

The susceptibility $\chi_e(\omega)$ is then used to calculate the dielectric function $\epsilon(\omega) = 1 + 4\pi\chi_e(\omega)$. The induced macroscopic polarization is related to the average induced current density, $\delta\mathbf{j}(\mathbf{r}, \omega)$ according to

$$\mathbf{P}_{\mathrm{mac}}(\omega) = \frac{i}{\omega V}\int_V d\mathbf{r}\,\delta\mathbf{j}(\mathbf{r}, \omega). \tag{6}$$

Within time-dependent linear response theory, we obtain the following relation for the induced density:

$$\delta\rho(\mathbf{r}, \omega) = \int\left(\frac{i}{\omega}\chi_{\rho\mathbf{j}}(\mathbf{r}, \mathbf{r}', \omega)\cdot\mathbf{E}_{\mathrm{mac}}(\omega) + \chi_{\rho\rho}(\mathbf{r}, \mathbf{r}', \omega)\delta v_{\mathrm{eff}}(\mathbf{r}', \omega)\right)d\mathbf{r}'. \tag{7}$$

The various Kohn–Sham response functions can be obtained from the occupied (i) and virtual (a) states of the ground-state system. They can be evaluated using the general form

$$\chi_{ab}(\mathbf{r}, \mathbf{r}', \omega) = \frac{V}{4\pi^3}\sum_{i,a}\int d\mathbf{k}\,\frac{\mathbf{a}_{ia\mathbf{k}}(\mathbf{r})\mathbf{b}^*_{ia\mathbf{k}}(\mathbf{r}')}{\epsilon_{i\mathbf{k}} - \epsilon_{a\mathbf{k}} + \omega + i\eta} + \mathrm{c.c.}(-\omega), \tag{8}$$

by substituting for $\mathbf{a}_{ia\mathbf{k}}(\mathbf{r})$ and $\mathbf{b}_{ia\mathbf{k}}(\mathbf{r})$ either the transition density $\rho_{ia\mathbf{k}}(\mathbf{r}) = \psi^*_{i\mathbf{k}}(\mathbf{r})\psi_{a\mathbf{k}}(\mathbf{r})$ or the relativistic transition current $\mathbf{j}_{ia\mathbf{k}}(\mathbf{r})$, which is given by [3]:

$$\mathbf{j}_{ia\mathbf{k}}(\mathbf{r}) = \frac{-ic^2}{2c^2 - v_{\mathrm{eff}}(\mathbf{r})}\left(\psi^*_{i\mathbf{k}}(\mathbf{r})\nabla\psi_{a\mathbf{k}}(\mathbf{r}) - \left(\nabla\psi^*_{i\mathbf{k}}(\mathbf{r})\right)\psi_{a\mathbf{k}}(\mathbf{r})\right). \tag{9}$$

These response kernels do not show any singular behavior even though the Kohn–Sham gap vanishes in the case of semimetals, as can be shown in a $\mathbf{k}\cdot\mathbf{p}$ analysis [3]. Since we keep the macroscopic field fixed, and since, within the ALDA, the effective potential is a functional of the density alone, we can solve the set of response equations, Eqs. (4) and (7), self-consistently.

With the perturbing effective potentials now fully determined, the induced paramagnetic current density $\delta\mathbf{j}_p(\mathbf{r}, \omega)$ follows from

$$\delta\mathbf{j}_p(\mathbf{r}, \omega) = \int\left(\frac{i}{\omega}\chi_{\mathbf{jj}}(\mathbf{r}, \mathbf{r}', \omega)\cdot\mathbf{E}_{\mathrm{mac}}(\omega) + \chi_{\mathbf{j}\rho}(\mathbf{r}, \mathbf{r}', \omega)\delta v_{\mathrm{eff}}(\mathbf{r}', \omega)\right)d\mathbf{r}'. \tag{10}$$

The total induced current contains, apart from this paramagnetic term, also the diamagnetic contribution, $\delta\mathbf{j}_d(\mathbf{r}, \omega) = (1/c)\rho_0(\mathbf{r})\mathbf{A}(\mathbf{r}, \omega)$. In the special case in which we choose the macroscopic field along one of the Cartesian directions μ, and with a frequency dependence according to $\mathbf{E}_{\mathrm{mac}}(\omega) = -i\omega\mathbf{e}_\mu$, the diamagnetic contribution to the current density reduces to $\delta\mathbf{j}_d(\mathbf{r}, \omega) = -\delta\mathbf{j}_p(\mathbf{r}, 0)$, i.e., to minus the static paramagnetic value [1]. The paramagnetic and diamagnetic components together form the total current, of which the average value yields the macroscopic polarization. For isotropic crystals the susceptibility now follows from

$$\chi_e(\omega) = \frac{-1}{3V\omega^2}\sum_\mu\int d\mathbf{r}\left[\delta\mathbf{j}_p(\mathbf{r}, \omega) - \delta\mathbf{j}_p(\mathbf{r}, 0)\right]_\mu\Big|_{\mathbf{E}_{\mathrm{mac}}(\omega) = -i\omega\mathbf{e}_\mu}, \tag{11}$$

where the index μ again labels the three Cartesian components.

Results and Discussion

The optical response calculations on HgSe were performed using the full-potential ADF-BAND package [1, 18, 19]. For both the ground state and the response calculations we used the free-atom core and valence orbitals, which were supplemented with Slater-type functions to form a triple-zeta valence basis. The free atom orbitals were obtained numerically using a Herman–Skillman type of program [20] employing the same ZORA approximation in the relativistic case. We kept the deepest core levels frozen and orthogonalized the valence basis to these cores, but the shallow 5d quasi-core states of Hg were included in the valence set. This basis was then further augmented using a double-zeta polarization set. All matrix elements were evaluated numerically with a relative accuracy of 1×10^{-3}. For the numerical evaluation of $\mathbf{k}$-space integrals, 175 symmetry-unique points were used to sample the irreducible wedge of the Brillouin zone. As lattice

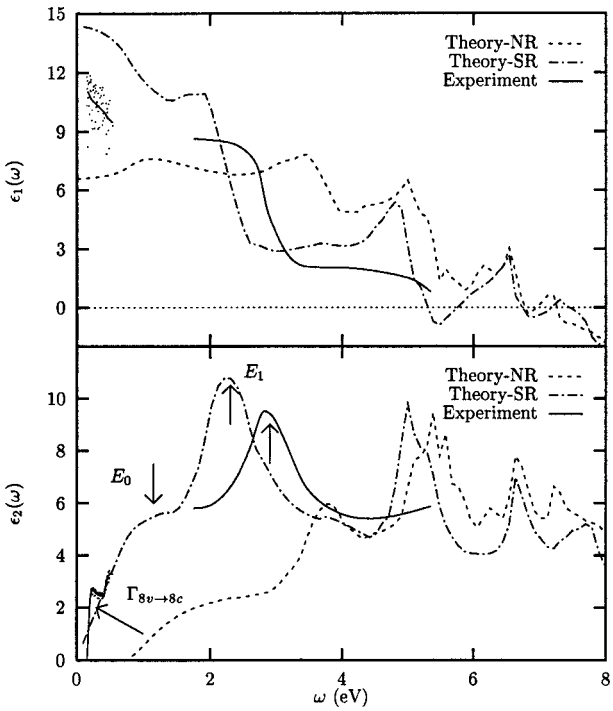

FIGURE 1. Plots of the real (top) and imaginary part (bottom) of the calculated dielectric function of HgSe with (SR, dash-dotted line) or without (NR, dotted line) including scalar relativistic effects. The experimental data have been compiled from Refs. [6, 21] (dots and solid line, for discussion see text).

parameter of the HgSe zinc blend structure we used $a = 6.08$ Å.

The experimental optical data compiled in Ref. [6] have been used to derive the low-frequency behavior for the dielectric function of HgSe. The room temperature refractive index data, which show a large scatter, were used in the frequency range above 0.2 eV to fit a quadratic polynomial in a least squares procedure (Fig. 1). In this range both the temperature dependence and the intraband contributions due to impurity carriers are small [6]. This refractive index measurements together with the absorption coefficients obtained at 5 K [6], provided the data to derive the experimental dielectric function in the infrared frequency range from 0.2 to 0.55 eV. We thus find an extrapolated value of 11.7 for the dielectric constant ϵ_∞. For the optical and ultraviolet frequencies we used ellipsometric data [21] in the range from 1.75 to 5.35 eV.

In Figure 2 we have depicted the energy dispersion of the highest valence and lowest conduction bands of HgSe. These band structures are shown for the two cases where we either included or excluded the relativistic effects. We can clearly see that the small direct gap at the center of the Brillouin zone Γ is reduced, and even inverted, upon inclusion of the scalar relativistic effects. The *s*-like (6*s* Hg) states at the conduction band minimum are stabilized with respect to the *p*-like (4*p* Se) states at the valence band maximum mainly due to the relativistic mass–velocity effect near the nucleus of Hg. This inversion of the typical band order [22] of zinc-blend-type semiconductors results in an avoided crossing, even at high symmetry directions, since the *s*-like band hybridizes with one of these *p*-like bands into Γ_{6v}. This results in an inverted gap of about -1.16 eV, which overestimates the experimental value of -0.45 eV by about 0.8 eV [6]. A further inclusion of spin-orbit coupling will split the *p*-like Se bands into an occupied $p_{1/2}$ band (Γ_{7v}) about 0.3 eV [7] below a half-occupied $p_{3/2}$ degenerate pair of bands (Γ_{8cv}), hence preserving the semimetallic nature of the band structure. This splitting will cause the Γ_{8cv} bands to be raised by about 0.1 eV (and the Γ_{7v} band to be lowered by about 0.2 eV), thus further increasing the inverted LDA gap to about -1.26 eV. This is in good agreement with the relativistic pseudopotential/LDA result (-1.27 eV) of Rohlfing and Louie [7], in which spin-orbit splitting was included. They found that quasiparticle (QP) corrections (within the GW approximation) mainly affect the *s*-like states, moving them upward rigidly by about 0.8 eV, thus reducing the gap $\Gamma_{6v} - \Gamma_{8cv}$ to about -0.51 eV. In the experimental optical spectra of HgSe, shown in Figure 1, this inverted gap appears as the critical point labeled E_0 at about

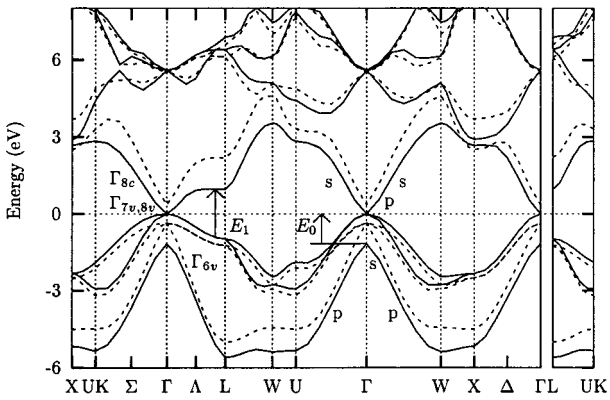

FIGURE 2. Inverted band structure of HgSe. The solid line is the result with scalar relativistic effects included. The dashed line is the nonrelativistic ground-state calculation. Critical points E_0 and E_1 and the band character (*s* or *p*) are indicated near the zone center Γ.

0.5 eV [6]. However, the absorption edge visible in the experiment at about 0.3 eV is most likely due to the transition between the bands connecting to Γ_{8v} and Γ_{8c}, which is symmetry forbidden at Γ, but becomes allowed outside this point since there Γ_{8c} changes character rapidly from p to s like. Simultaneous with the changing of Γ_{8c} the band connecting to Γ_{6v} changes from s to p character, while the bands connecting to Γ_{8v} and Γ_{7v} remain of p character. The quasi-particle shift of the s-like states will bring the s- and p-like bands closer together at Γ which will further enhance the steepness of the transition in character. This will allow for optical transitions of lower frequency, with a steeper edge in the absorption spectrum. The gap of about 1.95 eV between the nearly parallel top valence and lowest conduction band along the line Λ and at the point L at the zone boundary gives rise to the critical point E_1. This gap is again increased by about 0.80 eV when QP corrections are included. The top valence states $\Lambda_{4,5}$ along this line Λ will split by about 0.8 eV upon inclusion of spin-orbit coupling [22], but the bottom conduction band Λ_6 will not. This will give rise to a doublet structure in the dielectric function [6], which is however not clearly resolved experimentally at room temperature [21].

The TDDFT result for the dielectric function, depicted in Figure 1, shows a drastic change with the inclusion of the scalar relativistic corrections. We observe an almost fourfold increase in the absorption in the range from 1 to 3 eV, with a prominent E_1 feature just above 2.2 eV. The experimental E_1 peak appears around 3 eV. This shift is consistent with the underestimation of the energy gap along the line Λ in our grounds-state DFT-LDA calculation. Due to the Kramers–Kronig relation, the too low position of this peak will give rise to a too high calculated value for the dielectric constant $\epsilon_\infty = 14.4$, vs. 11.7 experimentally.

It is clear that with the removal of the energy gap, also the absorption onset has disappeared, although we do not reproduce the steep increase at the absorption edge $\Gamma_{8v} \rightarrow \Gamma_{8c}$. The E_0 critical point shows up as a knee in the calculation at around 1.25 eV (experimentally 0.45 eV), where again the relative shift of about 0.8 eV is in agreement with the overestimation of the $\Gamma_{6v} - \Gamma_{8c}$ gap in the ground-state calculation.

These relativistic effects are much larger than the contribution of the exchange and correlation effects. The magnitude of these xc effects in the response can be probed by excluding them in the response calculations. For both the relativistic and nonrelativistic calculation we get a featureless decrease of about 5% for the real part of the dielectric function for energies below the E_1 peak and virtually no change for frequencies above, whereas the reverse is observed for the imaginary part. In this last part we see no effects near the absorption edge, with a smooth crossover between the E_0 and E_1 peak to a uniform 5% decrease of the absorption for higher frequencies.

These findings are quite similar to the results we obtained previously for the InSb crystal [3]. There again the order of the energy bands is inverted at the point Γ within the local density approximation upon inclusion of relativistic effects. The interchanged s- and p-like character of the upper valence bands and the lowest conduction band switches back to the usual ordering just outside the zone center, along the same lines as in the analyses given above for HgSe. The inverted bandgap is much smaller than in HgSe; in InSb it is -0.42 eV, whereas in HgSe it is -1.26 eV. Experimentally, however, InSb is not found to be a semimetal but a narrow-gap semiconductor, with a direct gap of 0.23 eV [23]. A QP correction of 0.65 eV for the s-like band, similar to the rigid 0.8 eV energy shift for the s-like band in HgSe would revert the LDA band ordering in InSb again, resulting in a semiconducting band structure with the correct gap. Unlike the dispersion of the HgSe bands, in our LDA calculation for InSb both the lowest conduction band and the band connecting to Γ_{6v} have very strong dispersions, which hence corresponds to very low densities of states. We can therefore expect a very small contribution to the absorption at the E_0 critical point. We do not expect a possible QP correction similar to the HgSe case to severely modify the good overall agreement, even in the low-energy range. The original calculation resulted in a value of 16.4 for ϵ_∞ (15.7 experimentally [24]) and good overall agreement for the complete spectrum, which can be inferred by comparing the calculated dielectric function with the available experimental data [25], as depicted in Figure 3 of Ref. [3]. In conclusion, we showed that relativistic effects have a large contribution to the optical properties of the semimetal HgSe. The inverted band structure, which was recently debated, is also found in this ZORA-TDDFT calculation, for which the response calculation yields a dielectric function that is considerably improved compared to the nonrelativistic calculation, and is now in reasonably good agreement with experiment.

References

1. Kootstra, F; de Boeij, P. L.; Snijders, J. G. J Chem Phys 2000, 112, 6517.
2. Kootstra, F; de Boeij, P. L.; Snijders, J. G. Phys Rev B 2000, 62, 7071.
3. Kootstra, F; de Boeij, P. L.; Aissa, H.; Snijders, J. G. J Chem Phys 2001, 114, 1860.
4. Gawlik, K. U.; Kipp, L.; Skibowski, M.; Orlowski, N.; Manzke, R. Phys Rev Lett 1997, 78, 3165; Dietl, T.; Dobrowolski, W.; Kossut, J.; Kowalski, B. J.; Szuszkiewicz, W.; Wilamowski, Z.; Witowski, A. M. Phys Rev Lett 1998, 81, 1535; Gawlik, K. U.; Kipp, L.; Skibowski, M.; Orowski, N.; Manzke, R. Phys Rev Lett 1998, 81, 1536.
5. von Truchseß, M.; Pfeuffer-Jeschke, A.; Becker, C. R.; Landwehr, G.; Barke, E. Phys Rev B 2000, 61, 1666.
6. Einfeldt, S.; Goschenhofer, F.; Becker, C. R.; Landwehr, G. Phys Rev B 1995, 51, 4915.
7. Rohlfing, M.; Louie, S. G. Phys Rev B 1998, 57, R9392.
8. Bloom, S.; Bergstresser, T. K. Phys Status Solidi 1970, 42, 191.
9. Ekpenuma, S. N.; Myles, C. W. J Phys Chem Solids 1990, 51, 93.
10. van Lenthe, E.; Baerends, E. J.; Snijders, J. G. J Chem Phys 1994, 101, 9783.
11. van Lenthe, E.; van Leeuwen, R.; Baerends, E. J.; Snijders, J. G. Int J Quantum Chem 1996, 57, 281.
12. Philipsen, P. H. T.; van Lenthe, E.; Snijders, J. G.; Baerends, E. J. Phys Rev B 1997, 56, 13556.
13. Runge, E.; Gross, E. K. U. Phys Rev Lett 1984, 52, 997.
14. Hohenberg, P.; Kohn, W. Phys Rev B 1964, 136, 864.
15. Kohn, W.; Sham, L. J. Phys Rev A 1965, 140, 1133.
16. Breit, G. Phys Rev 1929, 34, 553; ibid 1932, 39, 616.
17. Vignale, G.; Kohn, W. Phys Rev Lett 1996, 77, 2037.
18. te Velde, G.; Baerends, E. J. Phys Rev B 1991, 44, 7888; J Comp Phys 1992, 99, 84.
19. Fonseca Guerra, C.; Visser, O.; Snijders, J. G.; te Velde, G.; Baerends, E. J. In Clementi, E.; Corongiu, G., Eds. Methods and Techniques in Computational Chemistry; STEF: Cagliary, 1995; p. 305.
20. Herman, F.; Skillman, S. Atomic Structure Calculations; Pretice-Hall: Englewood Cliffs, NJ, 1963.
21. Kumazaki, K.; Viña, L.; Umbach, C.; Cardona, M. Solid State Commun 1988, 68, 591.
22. Cardona, M.; Christensen, N. E.; Fasol, G. Phys Rev B 1988, 38, 1806.
23. Ashcroft, N. W.; Mermin, N. D. Solid State Physics; Holt, Rinehart and Winston: New York, 1976.
24. Burstein, E.; Brodsky, H.; Lucousky, G. Int J Quantum Chem 1967, 1, 756.
25. Aspnes, P. E.; Studna, A. A. Phys Rev B 1983, 27, 985.